ELSEVIER

Journal of Alloys and Compounds 434–435 (2007) 394–399

Journal of ALLOYS AND COMPOUNDS

www.elsevier.com/locate/jallcom

Influence of initial phase composition on glass-forming ability of Co-based alloys

E.A. Chikina [a], N.P. Dyakonova [a], V.V. Molokanov [b], T.A. Sviridova [a,*]

[a] *Moscow State Institute of Steel and Alloys, Technological University, Leninsky pr. 4, 117936 Moscow, Russia*
[b] *Institute of Metallurgy and Materials Science, Russian Academy of Sciences, Leninsky pr. 49, 117911 Moscow, Russia*

Available online 6 October 2006

Abstract

The glass-forming ability depending on initial phase composition of soft-magnetic $Co_{70}Fe_2Mn_4Si_{14}B_9Mo_1$ and $Co_{68}Cr_3Fe_3B_{12}Si_{14}$ alloys has been studied. It was found that granules of $Co_{70}Fe_2Mn_4Si_{14}B_9Mo_1$ alloy have the best glass-forming ability which allows to use these granules as a crystal precursor of amorphous state, which is prone to rapid amorphization with minimum energy consumption both on quenching alloy and on mechanical processing in a ball mill.

Keywords: Amorphous materials; Amorphisation; High-energy ball milling; X-ray diffraction; Thermal analysis

1. Introduction

Bulk amorphous alloys can be obtained by different methods. Among these methods the most commonly used ones are rapid quenching from the liquid state and mechanochemical synthesis or processing in high-energy ball mill. In the mills the amorphous state depending on initial ingredients can be achieved with different rates. The amorphization proceeds faster if intermetallic compounds are used as initial components [1,2]. Moreover the amorphous state is unattainable on mechanical alloying of pure elements if target composition of amorphous alloy includes boron with content less than 20–30 at.%. It is due to drastic difference in mechanical properties of metals and metalloids [1,3,4]. In that case the application of mixture of some compounds (or pre-alloys) as an alternative to elements is, probably, the only method for amorphous phase (AP) to be obtained in the ball mill. Unfortunately, the criteria characterizing glass-forming ability (GFA) of intermetallic compounds with metalloids are not formulated so far.

It is well known that the phase composition depends on not only chemical composition but also on cooling rate. Therefore the aim of this work is to study the dependence of GFA on alloy phase composition and to find composition with maximum GFA with the soft-magnetic Co-based alloys with high GFA taken as example.

2. Experimental details

The ingot and rapidly quenched (RQ) granules of $Co_{70}Fe_2Mn_4Si_{14}B_9Mo_1$ (hereinafter "Co70") alloy as well as crystallized RQ ribbon of similar composition $Co_{68}Cr_3Fe_3B_{12}Si_{14}$ (hereinafter "Co68") were investigated. Pure elements (99.98%) were used to prepare the ingot of Co70 alloy that was melted in argon atmosphere in an arc furnace and then chilled with cooling rate $\sim 10^2$ K/s. Some part of the ingot was used to produce RQ granules of size 160–250 and 250–400 μm by INROWASP method (cooling rate $\sim 10^3$ and $\sim 5 \times 10^2$ K/s, respectively). Other part of the ingot was used to obtain RQ amorphous ribbon by melt-spinning. RQ amorphous ribbon of Co68 alloy was annealed in vacuum at 650 °C during 1 h to complete crystallization.

Both the rate and completeness of amorphization in the course of mechanical milling (MM) were used as measures of GFA together with the value of melt undercooling determined by the differential thermal analysis (DTA). High-energy planetary ball mill of AGO-2U type was applied for MM, the milling time varied from 15 min to 12 h, ball-to-powder ratio was 200:20 g. Argon atmosphere was used for MM and sampling in the course of milling.

X-ray diffraction (XRD) patterns were obtained with Co Kα-radiation using step scanning DRON-4 diffractometer. While analyzing the samples with large AP content the modification of Rietveld full profile fitting method [5] was employed with addition of experimental X-ray pattern of the pure AP reference (RQ ribbon) rescaled into theoretical units of intensity [6]. The Fe-contamination due to abrasion of milling tools (steel balls) was checked by X-ray fluorescent method and amounted to some atomic percents.

The melt undercooling $\Delta T = T_m - T_S$ (where T_m and T_S are melting point and melt solidification temperature) was measured by high-temperature analysis in pure argon atmosphere. The sample under study was subjected to cycling in the temperature range from melting to solidification with consecutive elevation

* Corresponding author.
E-mail address: tim-17@yandex.ru (T.A. Sviridova).

0925-8388/$ – see front matter © 2006 Elsevier B.V. All rights reserved.
doi:10.1016/j.jallcom.2006.08.309

of melt temperature from cycle to cycle. Heating rate was 1.67 K/s, rate of melt cooling −9 K/s (cooling by switching off furnace), exposure at maximum temperature was 1 min.

Thermal analysis was carried out using high-temperature analyzer and calorimeter Setaram DSC-111.

3. Results

Fig. 1 shows X-ray diffraction (XRD) patterns of alloys in initial state and their phase identification. The crystallized ribbon consisted of Co_2B (struct. type C16), Co_2Si (struct. type C37), triple cubic boride $Cr_2Co_{21}B_6$ (struct. type $Cr_{23}C_6$). The phase composition of ingot and granules of alloy Co70 was only partially determined. The reliably identified phase constituents of ingot were cubic and hexagonal Co modifications (type A1 and type A3) and boride Co_2B (type C16). In addition to these constituents the ingot contained at least one unidentified phase, most likely, a silicon compound. The granules regardless of their size contained the same crystalline phases as the ingot except for boride Co_2B. In contrast with ingot, granules contained AP already in initial state and its volume fraction correlated with granules size.

Fig. 2 illustrates XRD patterns, which were obtained after ball milling with increasing time. As processing time grows,

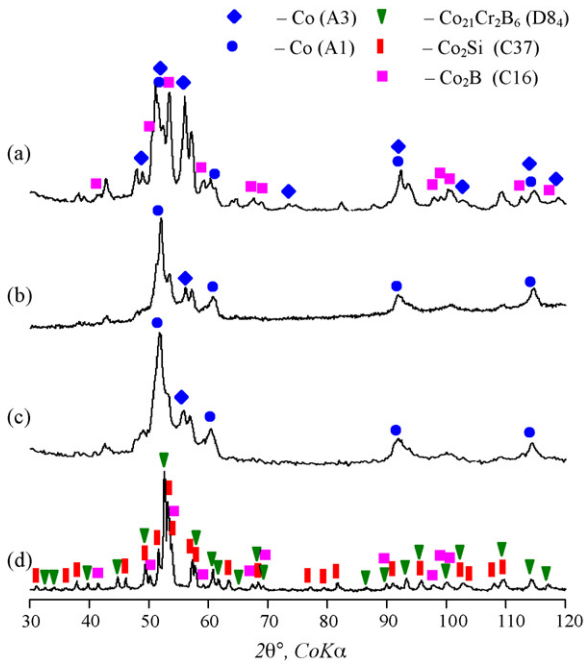

Fig. 1. X-ray diffraction patterns and phase composition of: (a) ingot of Co70 alloy; (b) granules of Co70 alloy of size 160–250 μm; (c) granules of Co70 alloy of size 250–400 μm; (d) crystallized ribbon of Co68 alloy.

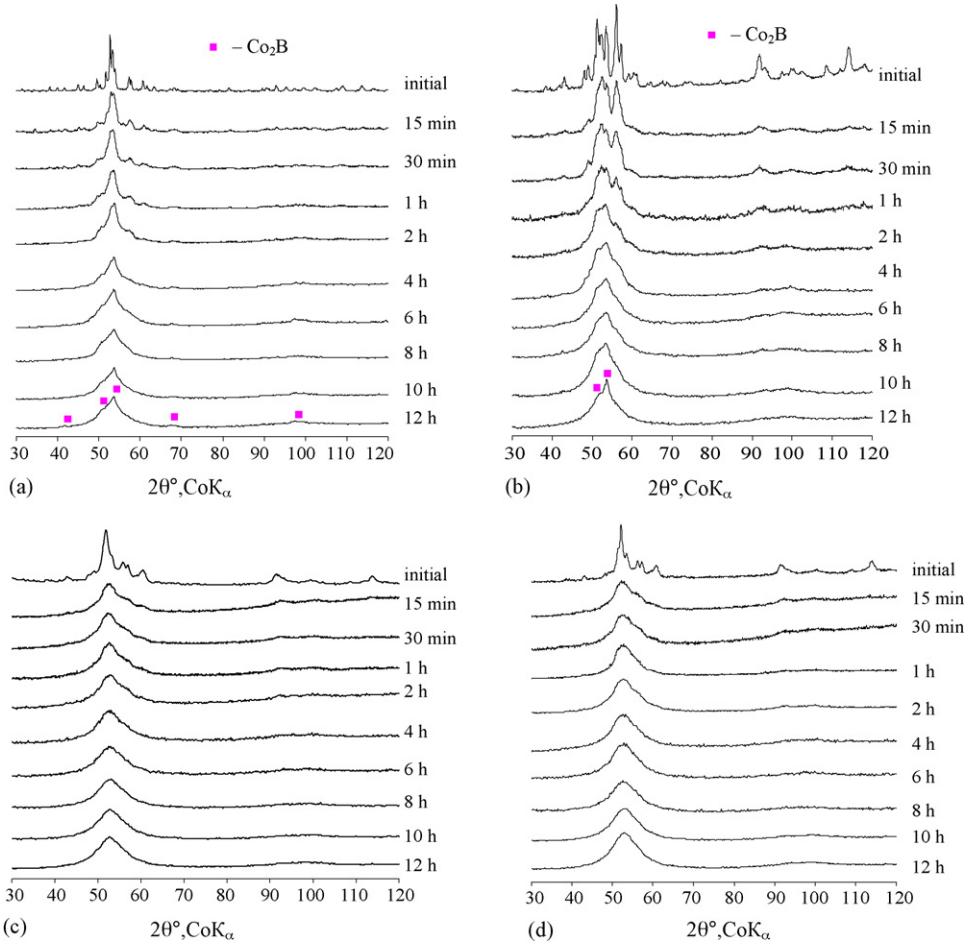

Fig. 2. X-ray patterns of samples after different milling time: (a) crystallized ribbon of Co68 alloy; (b) ingot of Co70 alloy; (c) granules of Co70 alloy of size 160–250 μm; (d) granules of Co70 alloy of size 250–400 μm.

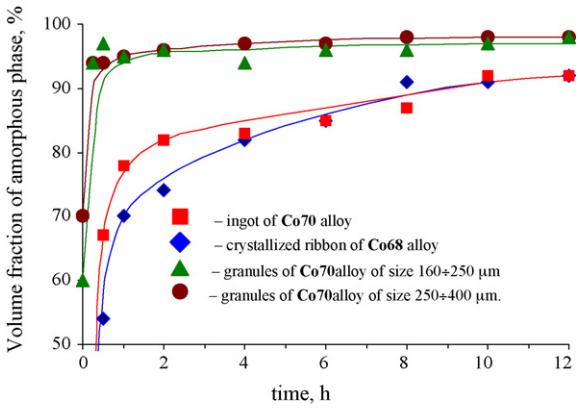

Fig. 3. Amorphization kinetics of samples under study.

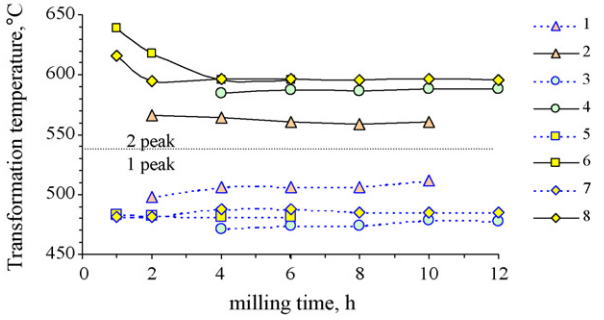

Fig. 4. Dependence of transformation temperatures (dotted and solid lines mean first and second peaks maxima respectively) in the course of DTA on milling time in different samples: (1 and 2) crystallized ribbon of Co68 alloy; (3 and 4) ingot of Co70 alloy; (5 and 6) granules of Co70 alloy of size 160–250 μm; (7 and 8) granules of Co70 alloy of size 250–400 μm.

the broadening of crystalline diffraction peaks and elevation of amorphous diffuse halo intensity take place in all samples. When granules are processed, peaks of crystalline phases practically disappear after 4 h of milling, whereas in the case of ingot the peaks of crystalline phase Co_2B remained after 12 h. The unidentified crystalline phase which was found in the ingot and granules of alloy Co70 proved to be unstable and decomposed after milling for 15–30 min. With this unknown phase vanished, the quantitative phase analysis became feasible which allowed to estimate the AP content and to study the kinetics of amorphization.

Fig. 3 shows dependence of AP content on milling time. The amorphization proceeded most quickly and completely in granules of Co70 alloy. Presumably, it can be attributed to specific composition of initial state, namely, AP presence and absence of Co_2B. The granules of different size are practically identical with regard to amorphization kinetics.

When the ingot Co70 and crystallized ribbon of Co68 alloy are processed, the transition into amorphous state proceeds slower and is not completed even after 12 h of milling. The crystalline phase Co_2B is still retained both in ribbon and in ingot as judged from XRD data. This boride is rather stable compound and is not disposed to amorphization or dissolution in the forming AP.

DTA data for alloys after different milling time are consistent with XRD results. Crystallization of AP, when present in the sample, proceeds in two stages. Fig. 4 shows how the temperatures of maxima for respective transformations shift with milling time. It can be seen that heat peak temperatures stabilized as time increased and after 4 h they were almost fixed. Inasmuch as the temperatures of AP crystallization stages depend on chemical composition, such stabilization signifies the completion of solid-state reactions induced by milling. This conclusion is in accordance with amorphization kinetics data (Fig. 3).

The results of DSC analysis of RQ ribbon and powders milled for 12 h are presented in Table 1 and in Fig. 5. As for AP in Co70 alloy, the ribbon, on the one hand, and all milled samples, on the other, display the most noticeable divergence in temperatures of crystallization stages. Both RQ ribbon and milled powders of Co70 alloy have very close temperatures of crystallization onset, whereas the temperature T_{p2} (corresponding to maximum of second transition) in RQ ribbon is approximately 30° higher than in milled samples. The difference between ribbon and powders in heat effect of crystallization can be attributed to distinction in geometric form of these samples.

The granules, being amorphous when milled for 12 h, are distinguishable from RQ ribbon by one more characteristic—the width of diffuse halo. The halo integrated width is taken here as a measure of AP imperfectness or heterogeneity. This value in granules equals 12.3° in comparison with 11.4° for RQ ribbon (in 2θ). As for Co68 alloy, the temperatures of crystallization in powder milled for 12 h also differ from ones in RQ ribbon. The temperatures of all crystallization stages in RQ ribbon are 60–80°C higher than in milled powder. The halo are also different, being equal to 10.8° and 12.8° for ribbon and powder, respectively.

Table 1
Transformation temperature and heat effects after different treatments

No.	Alloy and treatment	T_{x1} (°C)	T_{p1} (°C)	T_{p2} (°C)	ΔH (J/g)
1	Amorphous RQ ribbon of Co70 alloy	434	456	594	56
2	Granules of Co70 alloy (250–400 μm), 12 h of MM	431	463	565	43
3	Granules of Co70 alloy (160–250 μm), 12 h of MM	421	455	561	48
4	Ingot of Co70 alloy, 12 h of milling	425	453	554	43
5	Crystallized RQ ribbon of Co68 alloy, 12 h of MM	441	486	528	62
6	Amorphous RQ ribbon of Co68 alloy	500	514	590	57

T_x: temperature of transformation onset; T_{p1} (T_{p2}): corresponding peak (1 or 2) position in DTA curves; ΔH: total heat effect of first and second stages.

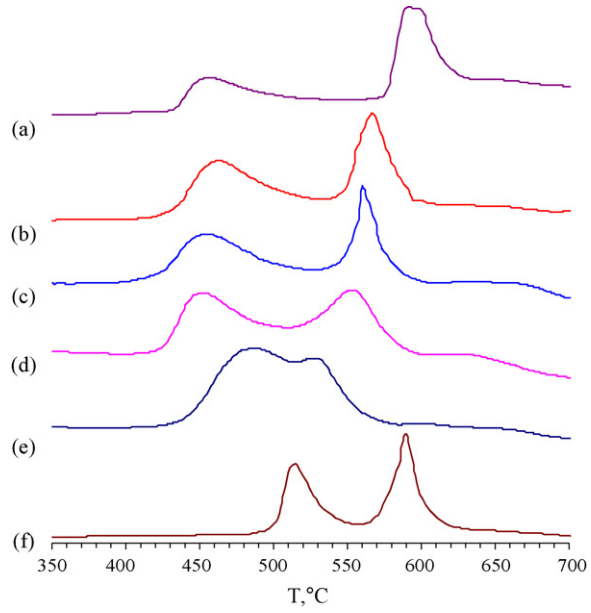

Fig. 5. DSC curves of different samples: (a) amorphous RQ ribbon of Co70 alloy; (b) granules of Co70 alloy 250–400 μm in size after 12 h of MM; (c) granules of Co70 alloy 160–250 μm in size after 12 h of MM; (d) ingot of Co70 alloy after 12 h of MM; (e) crystallized RQ ribbon of Co68 alloy after 12 h of MM; (f) amorphous RQ ribbon of Co68 alloy.

As it follows from Fig. 5, crystallization in all samples is a two-step process. To study the crystallization in more details, parts of samples were heated up to temperature corresponding to the end of first or second crystallization stage. Fig. 6 shows the XRD patterns and phase composition of the samples prepared differently from both alloys and then annealed in such a manner. The patterns for granules of size 250–400 μm are not shown because they are identical to the patterns of small-sized granules.

It is seen from the data presented that crystallization in differently prepared samples of Co70 alloy proceeds in dissimilar manner. The most essential distinction is revealed at the first crystallization stage. In amorphous RQ ribbon at first stage fcc phase with lattice parameter of pure cobalt precipitates (evidently, the phase has preferred orientation) accompanied by the bcc phase with $a = 0.2866$ nm, whereas the only crystalline phase in milled samples is bcc-phase with lattice parameter in the range 0.2814–0.2829 nm. In addition to bcc-phase, the ingot contains traces of compound Co_2B, which remains in the powder after milling. The phase composition of amorphous RQ ribbon at the second crystallization stage is identical to that of granules and ingot. It is interesting that phase composition in granules and ingot after crystallization differ markedly from their original phase composition before milling.

The crystallization of milled crystallized RQ ribbon of Co68 alloy also proceeds in two stages and some variations may be due to another chemical composition. At the first stage the bcc-phase precipitates from amorphous matrix and, along with it, traces of boride Co_2B formed on milling and survived when being then annealed. At the second stage the bcc-phase turns into stable compounds Co_2Si and boride $(Co,Me)_{23}B_6$ (struct. type $D8_4$) and also β-Co. The phase composition after second stage of crystallization practically coincides with that of original crystallized RQ ribbon before milling.

The melt undercooling was investigated as function of phase composition. The results are presented in Fig. 7. The temperature T_q from which the melt was quenched and temperature T_S of melt's solidification on cooling are plotted along horizontal and vertical axes. The dotted line plotted in Fig. 7 corresponds to alloy's melting point T_m. The melts produced from ingot and granules reveal maximum of undercooling ability in the T_q-regions I and II, respectively (see Fig. 7), i.e. at such T_q where T_S noticeably decreases. The undercooling ability may serve as a measure of GFA. The experiment demonstrated that melt produced from granules has the greater undercooling ability than melt derived from ingot as it has lower T_S at all T_q. Moreover

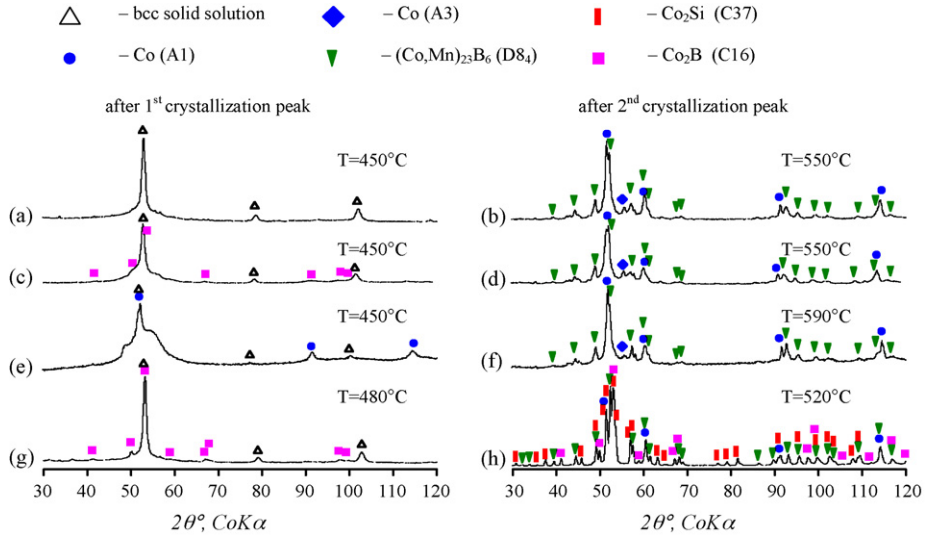

Fig. 6. X-ray patterns of samples after first and second crystallization peaks (heating temperatures are presented in picture): (a and b) granules of Co70 alloy (250–400 μm) after 12 h of MM; (c and d) ingot of Co70 alloy after 12 h of MM; (e and f) amorphous RQ ribbon of Co70 alloy; (g and h) crystallized RQ ribbon of Co68 alloy after 12 h of MM.

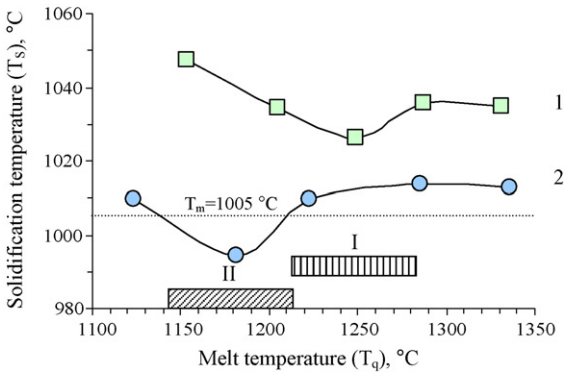

Fig. 7. The melt undercooling of $Co_{70}Fe_2Mn_4Si_{14}B_9Mo_1$ alloy: (1) ingot and (2) granules 250–400 μm in size.

the T_q-range at which the melt is able to be undercooled shifts by about 80 °C to lower values when passing from one melt to another (melted ingot and melted granules).

4. Discussion

As mentioned above, in this work GFA was estimated by two characteristics—rate of transition into amorphous state on MM and the melt undercooling ability. In the case of milling it is obvious that granules have a higher GFA and their size practically does not influence on it. The small GFA is inherent in all alloys, which contain the boride Co_2B (type C16) in initial state. Inasmuch as phases with this structure in the all previous studies [8,10] behaved analogously, its high stability may be related to the presence of especial atomic configurations in the phase (boron atoms positioned at very close distance, what is typical for stable and refractory borides).

However, as regards samples studied, in the most advantageous case of Co70 granules to be milled, the AP obtained by MM is not similar to that prepared by RQ. AP produced on milling, when being compared with that obtained by RQ, is characterized by lower temperature of second transformation and larger width of diffuse halo. Probably, it is accounted for by insufficient chemical heterogeneity of AP produced by MM. It may be supposed that increase of milling time allows to reach the state which is identical to that provided by RQ.

Crystallization mechanisms of ingot of Co70 alloy and crystallized ribbon of Co68 alloy varied from ones of amorphous ribbons because their had different chemical composition of amorphous phases which related with incomplete amorphization during MM.

In order to explain the relation between undercooling and phase composition it is necessary to suggest that different types of liquids coexist in the melt. This statement agrees with [7], where by measuring alloy's density it was proved the existence of high temperature and low temperature liquids. The difference between liquids of the same composition may be only in short-range order. This is confirmed by [7], where various phase content was fixed depending on melt quenching temperature. The greatest GFA is achieved if melt is quenched from temperature of "polymorphous transformation" in liquid.

The granules of Co70 alloy have been obtained by melt quenching from temperature region with maximum GFA and with cooling rate somewhat below the critical one. As a result, the multiphase state with metastable phases was "frozen" in granules. The part of these metastable phases should have short-range order similar to that in liquid, because the appearance of non-equilibrium phases is promoted by kinetics factors. These phases may be related to glass-forming compounds [8,9] as their presence in the alloy lead to increasing of GFA.

When alloy is heated by 100–200 °C above the melting point the melt inherits short-range order from constituent alloy crystalline phases. The similarity of crystalline short-range order to that of liquid with high GFA lead to increasing of undercooling ability.

However, owing to the fact that granules have an especial phase composition and do not contain refractory borides, the increasing undercooling ability (T_S drop) is accompanied by shift of region where the melt can be undercooled to lower temperatures (T_q drop). The liquid derived by melting of stable compounds which are formed when being cooled with a lower rate, contain stable atomic configurations with other short-range order. Such liquid takes on the most undercooling ability when alloy is quenched from temperature region at the boundary of low- and high-temperature liquids. Usually these temperatures exceed the melting point by 250–300 °C.

5. Conclusion

The glass-forming ability of soft-magnetic Co70 and Co68 alloys in dependence on phase composition was studied in this work. The variation of alloy's phase composition was attained by changing cooling rates and melt quenching temperature and also by crystallization of rapidly quenched ribbon.

The GFA was estimated by two methods: (1) time and completeness of amorphization on MM; (2) melt undercooling ability. It was established that the granules of Co70 alloy obtained by rapid quenching with the rate 5×10^2 to 10^3 K/s from the optimal temperature have the greatest glass-forming ability.

The amorphous phases obtained by ball milling and rapid quenching were compared as regards to their transition temperatures, crystallization mechanisms and width of diffuse halo. It was found that amorphous phase produced by mechanical milling of granules of Co70 alloy was the most similar to that obtained by melt quenching, what can be explained by absence of stable boride Co_2B.

Thus, the feasibility of fast amorphization is determined by initial phase composition of preliminary prepared crystalline sample or so called *precursor* of amorphous phase. The use of rapidly quenched precursor with metastable amorphous-crystalline structure that does not contain refractory borides facilitates amorphization. Such a precursor secures the fastest transition to amorphous state by either rapid quenching or processing at high-energy ball mill with minimum energy consumption.

Acknowledgement

This work was partially supported by Russian Foundation for Basic Research RFBR (Grants No. 04-03-32700).

References

[1] V.V. Molokanov, A.N. Shalygin, M.I. Petrzhik, T.N. Mikhailova, K.S. Filippov, N.P. D'yakonova, T.A. Sviridova, E.A. Zakharova, J. Adv. Mater. 10 (1) (2003) 5–13.
[2] N.P. Djakonova, T.A. Sviridova, E.A. Zakharova, V.V. Molokanov, M.I. Petrzhik, J. Metastable Nanocryst. Mater. 15–16 (2003) 673–678.
[3] J. Jing, A. Calka, S.J. Campbell, J. Phys. Condens. Matter 3 (1991) 7413.
[4] K. Omuro, H. Miura, H. Ogawa, Mater. Trans. JIM 36 (2) (1995) 258–262.
[5] E.V. Shelekhov, T.A. Sviridova, Met. Sci. Heat Treatment 42 (7) (2000) 309–313.
[6] E.V. Shelekhov, T.A. Sviridova, Materialovedenie No. 10 (1999) 13–22.
[7] V.V. Molokanov, A.N. Shalygin, M.I. Petrzhik, T.N. Mikhajlova, K.S. Filippov, V.I. Kashin, T.A. Sviridova, N.P. D'yakonova, Perspekt. Mater. 3 (2003) 10–17.
[8] M.I. Petrzhik, V.V. Molokanov, Izv. RAN, ser. Phys. 65 (10) (2001) 1384–1389 (Russian).
[9] N.P. Djakonova, T.A. Sviridova, E.A. Zakharova, V.V. Molokanov, M.I. Petrzhik, J. Alloys Compd. 367 (1–2) (2004) 191–198.
[10] M.A. Vorgol'skya, N.P. Dyakonova, T.A. Sviridova, T.R. Setdekova, V.V. Molokanov, Abstracts of Conference "Structural foundations of materials modification by non-traditional technology MNT-7", Obninsk (2003) 29–31 (in Russian).